PZT Actuated Four-Bar Mechanism with Two Flexible Links for Micromechanical Flying Insect Thorax

Metin Sitti
Dept. of EECS, University of California at Berkeley, CA 94720
sitti@eecs.berkeley.edu

Abstract

In this paper, a four-bar mechanism with two flexible links is proposed to be used in a micromechanical flying insect robot wing thorax design for stroke amplification. PZT-5H and PZN-PT based unimorph actuators are utilized at the input link of the four-bar. The kinematics and dynamics of the proposed wing strcuture with two parallel four-bar mechanisms are analyzed, and DC forces generated at the wing are computed for checking the feasibility of the design. Using laser micromachining and folding techniques, prototype four-bars are constructed, and it is shown that the single four-bar structure can have $90-100^o$ *stroke motion at* $29\ Hz$ *with a rigid polyester wing on it.*

1 Introduction

Being inspired from the biological mechanisms and structures in nature, human could innovate many novel technologies and devices from the early times. As a recent example of this, biomimetic robotics has been enabling novel devices and approaches to robotic problems. This kind of field would enable multifunctional, smart, suboptimal, nature friendly, complex and adaptive machines and devices. Flying insect robots are one of the important inspiration areas for the robotic researchers [1], [2], [3], [4] where high maneuverability and novel distributed intelligent device applications would become possible with mechanical flies. On the other hand, especially considering the design issue of a wing structure for a micromechanical flying insect (MFI) robot with sizes and performances comparable to a real fly, many new challenging design constraints are introduced in the respects of size, weight, motion speed, power consumption, biomimetic kinematics, space efficiency, etc. Therefore, light structures with high resonant frequencies, low power consuming and compact actuators, and high stroke and rotation motion mechanisms issues are the main challenges of this field.

This paper considers mainly the stroke amplification and compact actuator design issues using a four-bar mechanism with two flexible links and integrated PZT unimorph actuator at the input link. The detailed design and characterization of the unimorph actuators are given in [5]. For stroke amplification, different compliant mechanisms are proposed such that Pokines [6] proposed a microamplifier fabricated using LIGA process, Precht [7] developed a large stroke bender actuating a trailing edge flap, Kota *et al.* [8], [9] designed micro compliant mechanisms including a four-bar based mechanism, and Cox *et al.* constructed PZT bimorph [2] and unimorph [10] based flapping mechanisms with compliant flexures. However, these works do not have a detailed kinematic, dynamic and quasi-static blocking force analysis of the compliant mechanism for a specific task, and none of them could have a large stroke flapping mechanism for a micromechanical flying device (Cox *et al.* achieved $30-50^o$ flapping stroke). In this paper, detailed analysis is realized for a micromechanical flapping wing mechanism based on a compliant four-bar structure, and a high stroke flapping mechanism is developed. Furthermore, many design constraints are considered such that the proposed design enables a compact and light weight thorax, high torques at the wing, and high resonant frequency ($> 25\ Hz$).

2 Four-Bar Thorax Structure

The complete view of the wing structure to be constructed is shown in Figure 1. Two four-bar mechanisms constitute the parallel thorax structures that could enable targeted biomimetic $70-160^o$ stroke and 90^o wing rotation motions [11] with proper stroke amplification at resonant frequency of $100-150\ Hz$. This compact design assumes a flexible wing, and a fan-fold structure is proposed for this problem. The structure of the proposed four-bar mechanism with a wing spar on it is shown in Figure 2. Two elastic beams at the input and output links deflect with $\Delta\theta$ and $\Delta\psi$ angles so that the coupler link and spar rotate with angle ϕ. Then the stroke amplification N of the structure can be defined as:

$$N = \frac{\phi_{pp}}{\theta_{pp}} \tag{1}$$

where $\theta_{pp} = \theta_{max} - \theta_{min}$ and $\phi_{pp} = \phi_{max} - \phi_{min}$ are the peak-to-peak input and output link motions.

For the simplicity of the analysis, the input and output deflections are assumed to be linear, i.e. small, which is the case for PZT unimorph actuators with moderate input electric fields. Thus, the mechanism can be approximated by a four rigid link four-bar mechanism with four rotational (4R) pin joints. Therefore, the kinematics is

approximated with the rigid 4R kinematics [12] while the dynamics is characterized by utilizing the lumped modeling of the flexible beams as can be seen in Figure 3. For large motions of the unimorph flexible link, finite element methods can be utilized for more accurate dynamic modeling [13], [14].

In this proposed four-bar thorax design, if the generated stroke is under the target $70-160^o$ range due to the limitations in the unimorph actuator motion range and output torques, then the multiple four-bar structure as illustrated in Figure 4 can be constructed.

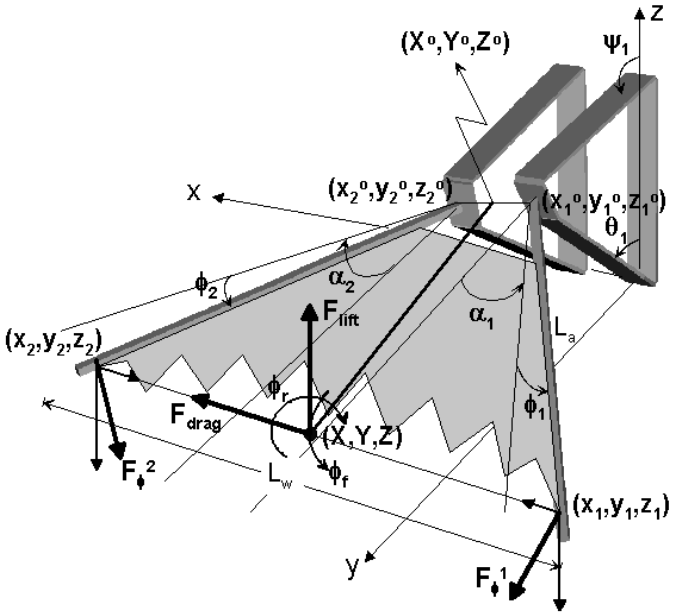

Figure 1: Proposed wing structure, and its kinematic and force parameters.

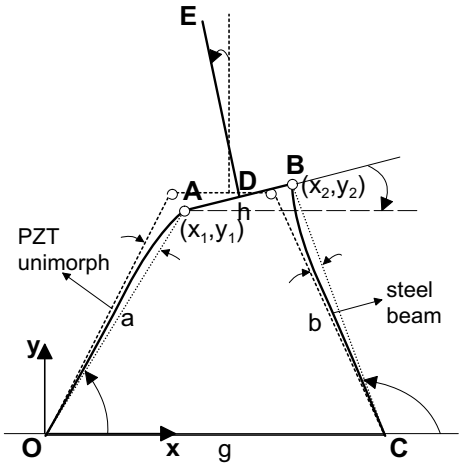

Figure 2: Four-bar mechanism with two elastic beams at the input (**OA**) and output (**BC**) links.

3 Wing and Thorax Kinematics

In order to provide a biomimetic kinematics at the wing, the forward and inverse kinematics of the wing shown in Figure 1 are analyzed. Assuming that two four-bar

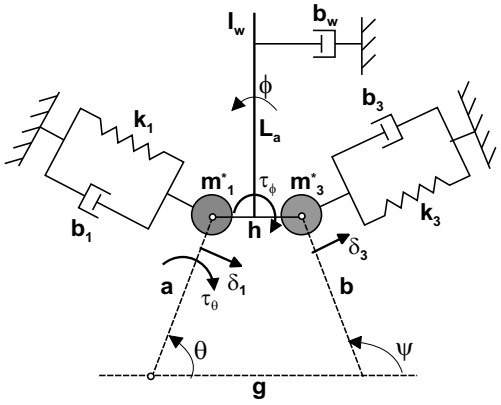

Figure 3: Lumped parameter dynamic modeling of the four-bar mechanism with two flexible beams, and a rigid spar load with an aerodynamic external force on it.

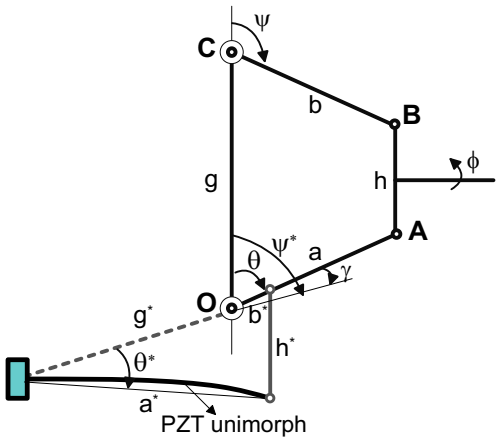

Figure 4: Multiple (two here) four-bar design proposal for enabling more stroke amplification if necessary.

mechanisms can be approximated as 4R rigid links, with pin joint mechanisms for simplicity, four-bar output angles ψ_1 and ψ_2 and wing spar rotations ϕ_1 and ϕ_2 can be computed from the input link rotations of θ_1 and θ_2 as (**Appendix 1**):

$$\begin{aligned} \phi_i &= tan^{-1}\Big(\frac{y_2-y_1}{x_2-x_1}\Big) \\ \psi_i &= tan^{-1}\Big(\frac{y_2}{x_2-g}\Big) \end{aligned} \tag{2}$$

Thus, the wing flapping and rotation angles ϕ_f and ϕ_r as illustrated in Figure 1 can be computed as

$$\begin{aligned} \phi_f &= tan^{-1}\Big(\frac{Z-Z^o}{\sqrt{(X-X^o)^2+(Y-Y^o)^2}}\Big) \approx \frac{\phi_1+\phi_2}{2} \\ \phi_r &= tan^{-1}\Big(\frac{z_1-z_2}{\sqrt{(x_2-x_1)^2+(y_2-y_1)^2}}\Big)\,. \end{aligned} \tag{3}$$

As the inverse kinematics, θ_1 and θ_2 input link motions are computed from the desired biomimetic ϕ_f and ϕ_r. At first, given ϕ_f and ϕ_r, the aim is to compute ϕ_1 and ϕ_2. From Eq. (3), it can be seen that ϕ_f and ϕ_r are coupled with θ_i and ϕ_i nonlinearly. Therefore, a closed

form solution is complex, and following simplifications can be made: (1) Assume that (x_1^o, y_1^o, z_1^o) and (x_2^o, y_2^o, z_2^o) is not a function of θ_i, i.e. the base of the spars are not moving, (2) $(y_2 - y_1)^2$ term is negligible in the ϕ_r equation. Then,

$$tan\phi_r \approx \frac{z_1 - z_2}{x_2 - x_1} \tag{4}$$

Then, assuming $\alpha_1 = \alpha_2 = \alpha$, ϕ_i stroke angles, θ_i and ψ_i $i = 1, 2$ are computed in **Appendix 2**.

For testing the approximation error for the inverse kinematics equations, an insect biomimetic trajectory for $\pm 45^o$ wing flapping and 90^o rotation is used as the desired ϕ_f and ϕ_r as shown in Figure 5c [11]. The resulting inverse kinematics solutions in the reference four-bar actuator motions of θ_1 and θ_2, and spar stroke motions of ϕ_1 and ϕ_2 are shown in Figure 5a and 5b. Parameters of the thorax are $a = 5\ mm$, $b = 3\ mm$, $g = 4.5\ mm$, $h = 0.5\ mm$, $L_t = 1\ mm$, $L_a = 7\ mm$, $\alpha = 30^o$, and motion bandwidth 100 Hz. By using the forward kinematic equations, computed θ_i and ϕ_i values are used for computing the ϕ_f and ϕ_r at the wing. As given in Figure 5c, it can be seen that the simplification in Eq. (4) results in a small error, and therefore it can be used for generating the actuator reference motion.

3.1 Size Optimization

Using kinematics equations, optimal four-bar link sizes and initial angles are drived for optimal stroke amplification N. Fixing h and PZT input voltage V, the effect of $a = b = l$ and initial input link angle θ_0 on N is investigated. Here, $g = h + 2Lcos\alpha$ due to the symmetry. Maximum PZT deflection, i.e. maximum $\Delta\theta$, can be derived for a steel and PZT heterogenous unimorph actuator as [15]:

$$\begin{aligned} \Delta\theta &= 3d_{31}\frac{lAB}{K}V \\ K &= 4s_p s_s h_s h_p^3 + 4s_p s_s h_s^3 h_p + s_p^2 h_s^4 + \\ &\quad s_s^2 h_p^4 + 6s_p s_s h_s^2 h_p^2 \\ B &= \frac{h_s(h_s + h_p)}{s_p h_s + s_s h_p} \\ A &= s_s s_p (s_p h_s + s_s h_p)\ . \end{aligned} \tag{5}$$

where h_p and h_s are the thicknesses, and s_p and s_s are the vertical direction compliances of the piezoelectric and steel layers respectively, and d_{31} is the piezoelectric constant, V is the PZT actuator input voltage. For a PZT-5H piezoelectric layer, if $h_p = 70\ \mu m$, $h_s = 50\ \mu m$, $s_p = 2 \times 10^{-11}\ m^2/N$, $s_s = 5.18 \times 10^{-12}\ m^2/N$, $d_{31} = 274 \times 10^{-12}\ C/N$, $h = 0.5\ mm$ and $V = 150\ V$, ϕ_{pp} values could be seen in Figure 6. For large L, small α angles result in singularity while the optimal ϕ_{pp}, i.e. N, can be held close to the singularity.

4 Thorax Dynamics

Assuming the elastic beams are linearly bended with small δ_1 and δ_3 displacements, they are represented as

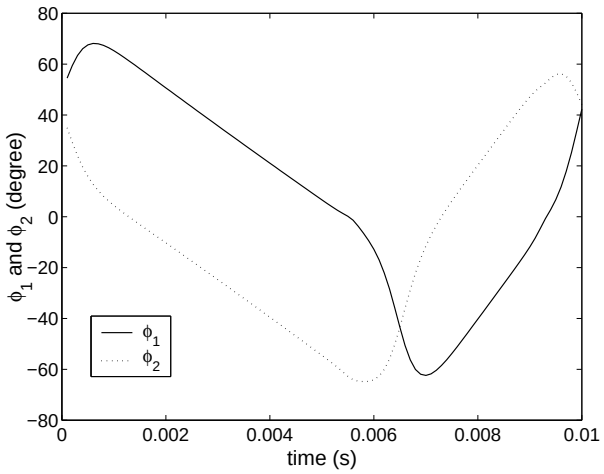

(a)

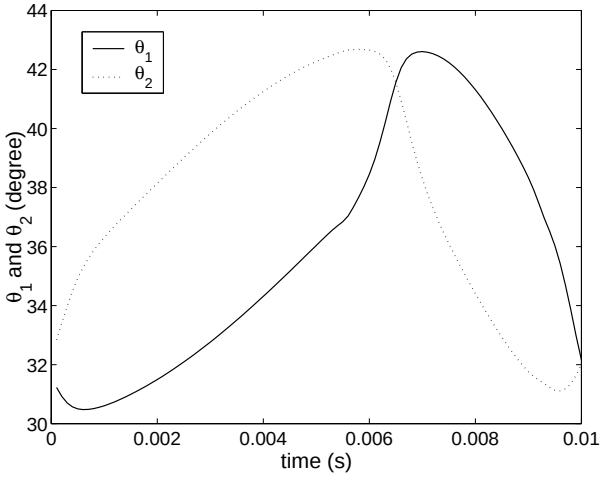

(b)

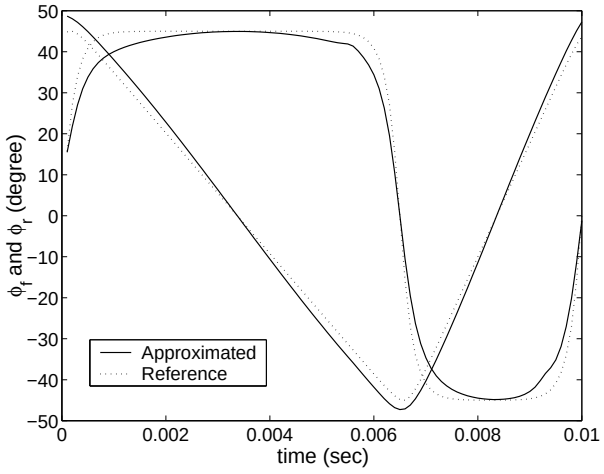

(c)

Figure 5: Inverse kinematics simulation for the wing for tracking a biomimetic kinematic motion: (a) computed stroke motions of ϕ_1 and ϕ_2; (b) computed four-bar input link motions of θ_1 and θ_2; (c) biomimetic reference (dotted lines), and approximated (solid lines) wing flapping and rotation motions.

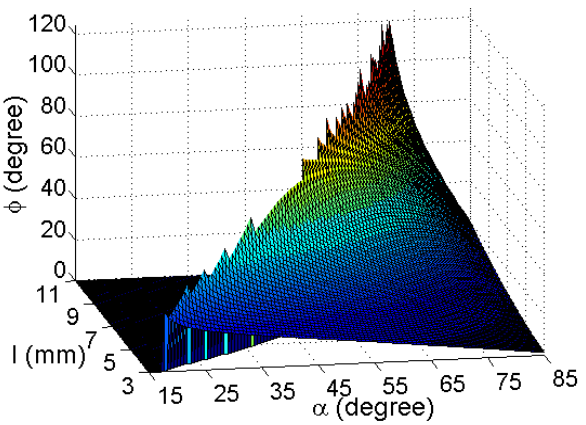

Figure 6: Stroke amplification as a function of the four-bar link sizes of $a = b = l$, and initial input link angle when $h = 0.5\ mm$ and input voltage $V = 150\ V$ are fixed ($\phi_{pp} = 0$ region corresponds to the singular values).

point effective masses of $m_1^* = 0.24m_1$ and $m_3^* = 0.24m_3$ with spring constants of k_1 and k_3, and damping coefficients of b_1 and b_3 as shown in Figure 3. The coupler is a rigid link with a long rectangular bar of mass m_s and length L_a. b_w in the figure represents the aerodynamic damping on the spar where $b_w = 0$ when there is no wing on the spar, and wing inertia $I_w = 0$.

The kinetic energy K, potential energy U and dissipation energy D are computed for the equation of motion derivation as [16]

$$\begin{aligned} K &= \frac{1}{2}m_1^*\dot{\delta}_1^2 + \frac{1}{2}m_3^*\dot{\delta}_3^2 + \frac{1}{2}I_2\dot{\phi}^2 + \frac{1}{2}m_2[a^2 + r_2w_2^2 + \\ &\quad 2aw_2r_2cos(\phi - \theta + \beta_2)]\dot{\theta}^2 = \frac{1}{2}A(\theta)\dot{\theta}^2 \\ U &= \frac{1}{2}k_1\delta_1^2 + \frac{1}{2}k_3\delta_3^2 + m_tgacos\theta + m_3^*ghcos\phi + \\ &\quad m_2gr_2cos(\beta_2 + \phi) \\ D &= \frac{1}{2}b_1\dot{\delta}_1^2 + \frac{1}{2}b_3\dot{\delta}_3^2 + \frac{1}{2}b_w\dot{\phi}^2 = \frac{1}{2}F_0\dot{\theta}^2\ . \end{aligned} \quad (6)$$

Using the Lagrange equation of

$$\frac{d}{dt}\Big(\frac{\partial K}{\partial\dot{\theta}}\Big) - \frac{\partial K}{\partial\theta} + \frac{\partial U}{\partial\dot{\theta}} + \frac{\partial D}{\partial\theta} = \tau_\theta \quad (7)$$

the following equation of motion is derived (**Appendix 3**):

$$A\ddot{\theta} + \frac{1}{2}\frac{dA}{d\theta}\dot{\theta}^2 + D_0 + D_1w_3 + D_2w_2 + F_0\dot{\theta} = \tau_\theta\ . \quad (8)$$

As approximate lumped estimates of the resonant frequency $\omega = 2\pi f_r$ and mechanical quality factor of the wing and thorax Q, following equlaties are derived:

$$\begin{aligned} \omega^2 &= \frac{k_1a^2 + w_3^2k_3b^2}{m_1^*a^2 + w_2^2I_2 + w_3^2m_3^*b^2} \approx \frac{k_1a^2 + w_3^2k_3b^2}{w_2^2I_2} \\ Q &= \frac{k_1a^2 + w_3^2k_3b^2}{\omega(b_1 + w_2^2b_w + w_3^2b_3)}\ . \end{aligned} \quad (9)$$

5 DC Force Analysis

In the thorax design, one important parameter is the generated torques (or lift forces) at the wing spars. If these torques are significantly less than the generated up or down lift forces by the aerodynamic forces, the designs will not give enough performance. Therefore, the computation of these forces for the proposed design is realized for performance evaluation.

Assuming the 4-bar input link is rotated by a small $\delta\theta$ by applying an input voltage V through the input link unimorph actuator, and the motion is quasi-static (DC motion), resulting spar motion $\delta\phi$ and blocking torque τ_ϕ have the following relation using the *principle of virtual work*:

$$\delta W_v = \tau_\theta\delta\theta + \tau_\phi\delta\phi = \delta U = k_1a^2\Delta\theta\delta\theta + k_3b^2\Delta\psi\delta\psi\ . \quad (10)$$

Here, the gravitational terms are neglected. For a constant δt, $\delta\phi = w_2\delta\theta$ and $\delta\psi = w_3\delta\theta$. Thus,

$$\tau_\theta + w_2\tau_\phi = k_1a^2\Delta\theta + k_3b^2w_3\Delta\psi\ . \quad (11)$$

Here, unimorph actuator tip torque τ_θ can be given as:

$$\tau_\theta = -aF_b = -\frac{3}{4}d_{31}wBV \quad (12)$$

where w is the unimorph width. For stiffnesses:

$$\begin{aligned} k_1 &= \frac{Kw}{4Aa^3} \\ k_3 &= \frac{wh_s^3}{4b^3s_s} \end{aligned} \quad (13)$$

Using above equations, the blocking torque at the spar end is computed as:

$$\tau_\phi = \frac{1}{w_2}(\frac{3}{4}d_{31}wBV + k_1a^2\Delta\theta + k_3b^2w_3\Delta\psi)\ . \quad (14)$$

The lift force on the i^{th} $(i = 1, 2)$ wing spar generated by the above torque can be computed as $F_\phi^i = \tau_\phi^i/L_a$. Then the average lift force and drag force at the wing rotation axis edge are:

$$\begin{aligned} F_{lift} &= -(F_\phi^1cos\alpha_1cos\phi_1 + F_\phi^2cos\alpha_2cos\phi_2)/2 \\ F_{drag} &= F_\phi^1sin\alpha_1sin\phi_1 - F_\phi^2sin\alpha_2sin\phi_2\ . \end{aligned} \quad (15)$$

Denoting the measured aerodynamic lift and drag forces as F_l and F_d, $F_{lift} \geq -F_l$ and $F_{drag} \geq -F_d$ equalities should be held at each instant for enabling sufficient forces for flight with any thorax and wing design.

6 Thorax Fabrication

Assembly process of the four-bar with spar is shown in Figure 7. Super glue is used for attaching a steel base to the unimorph for fixing it to the base frame, conductive epoxy is used for the cable connection to the unimorph actuator, and the unimorph ground cable is soldered to the steel beam. The top link joint is designed by a polyester flexible sheet of 12.5 μm thickness, and

is cut by a laser micromachining device. Fabrication result for PZT-5H and PZN-PT based unimorph actuators are displayed in Figure 8. In Figure 8b, a polyester wing with 100 μm thickness is also attached for flapping experiments.

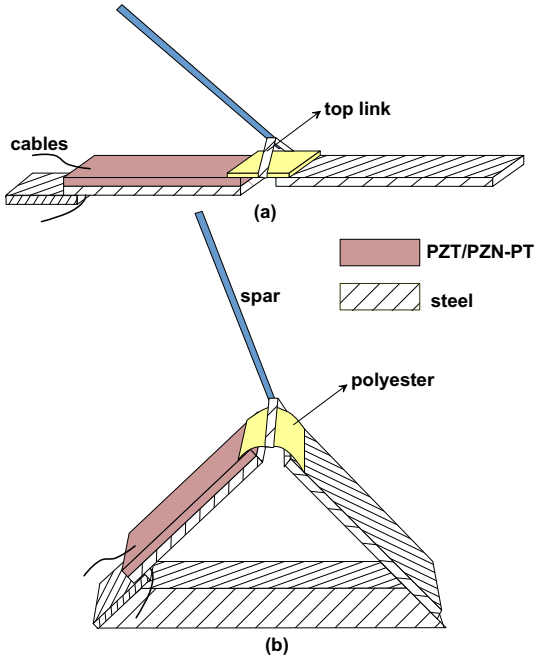

Figure 7: Assembly process of the unimorph and steel beam with polyester flexible joints: (a) horizontal assembly of input, output and top links and steel spar, (b) assembly with the hollow rectangular steel base.

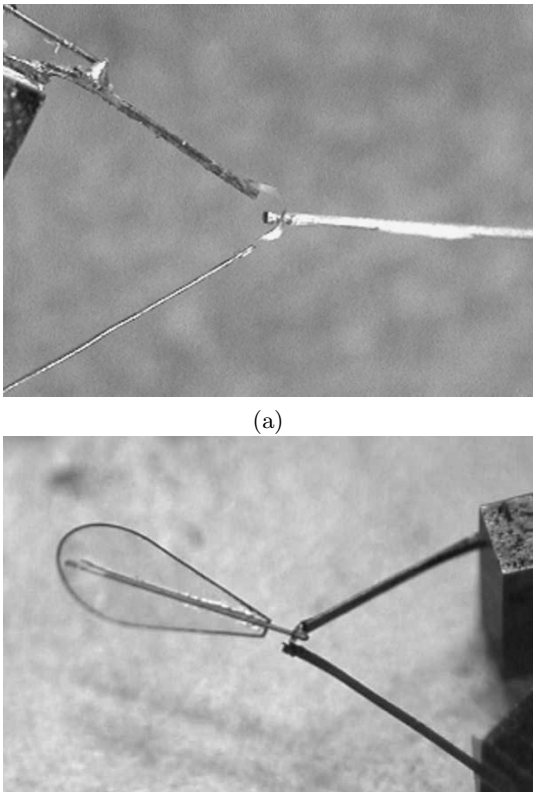

(a)

(b)

Figure 8: Fabrication results of unimorph and steel beam input and output links with polyester flexible joints assembly: (a) $5 \times 1 \times 0.25\ mm^3$ PZN-PT unimorph based four-bar and spar, (b) $10 \times 1 \times 0.12\ mm^3$ PZT unimorph based four-bar with a rigid polyester wing.

7 Simulation and Experiments

For the simulations of a four-bar mechanism with the bonded PZN-PT actuator and steel at the input link, the parameters are: $a = l = 5\ mm$, $w = 1\ mm$, $b = 3\ mm$, $g = 4.5\ mm$, $h = 0.5\ mm$, $L_a = 7\ mm$, $\alpha_1 = \alpha_2 = 30^o$, $L_t = 1\ mm$, $h_p = h_s = 50\mu m$, $s_p = 65 \times 10^{-12}\ m^2/N$, $s_s = 5.18 \times 10^{-12}\ m^2/N$, and $d_{31} = 950 \times 10^{-12}\ C/N$. Thus, $k_1 = 94.85\ N/m$, $k_3 = 48.26\ N/m$, $m_1 = 2.05\ mg$ and $m_3 = 1.9\ mg$. For these values input link DC motions are $\theta_1 = \theta_1^0 \pm 6^o$ and $\theta_2 = \theta_2^0 \pm 5.78^o$ with $\theta_1^0 = 36.54^o$ and $\theta_2^0 = 36.89^o$ as shown in Figure 9a. Then DC kinematic spar motions are given in Figure 9b. For different electric fields of $E_{1,2} \in [-5, 5]\ V/\mu m$, the range of actuator and spar torques, and lifting and drag forces are given in Figures 10 and 11 respectively. Since the aerodynamic lift force would be equal or twice the weight of the overall flying robot which is designed for overall weight of 1 mN [1], the aerodynamic loading would be in the range of $0.7 - 1.4 \times 10^{-5}\ Nm$ where the resultant torques in Figure 10 with the range of $[-5, 4] \times 10^{-5}\ Nm$ can handle this range of forces.

Next, the fabricated four-bar in Figure 8b without a wing at the beginning was tested. Motion of the spar for $\theta_{pp} = 4^o$ unimorph deflection is shown in Figure 12. Here $a = b = 10\ mm$, $h = 0.5\ mm$ and $V = \pm 150\ V$. The up and down strokes are also observed with an optical microscope as displayed in Figure 13. The spar has a stroke of $80 - 90^o$ at resonance of 32 Hz. This means $N \approx 22$ is achieved which is coinciding with the size optimization graph in Figure 6. On the other hand, from Eq. (9), $f_r = \omega/2\pi = 61\ Hz$ is estimated by the values of $k_1 = 43.7\ N/m$, $k_3 = 24.1\ N/m$, $Q_1 = 22$, $Q_3 = 35$, $m_1 = 9.4\ mg$, $m_3 = 3.9\ mg$, $I_2 = 1.14 \times 10^{-10}\ kgm^2$, $w_2 = 20$, and $w_3 = 1$. Here, the loss in the frequency is due to the neglected polyester flexure compliance. Then, the wing is attached and the motion of the four-bar is tested as displayed in Figure 14. The stroke motion becomes around $90 - 100^o$ with resonance at 29 Hz. This shows that the attached wing does not result in significant damping due to the aerodynamic forces (b_w in Figure 3). However, if the area and size of the polyester wing is increased more, at some point the aerodynamic damping would become significant.

Finally, dependency of N on θ_0 is tested experimentally for $a = b = L = 10\ mm$ for a small motion case ($V = 100\ V$). The plot of the N vs. the stroke amplitude (ϕ_{pp}) is shown in Figure 15a. Here, there are two optimal values of θ_0 where one is around 35^o and the other is around 70^o. The latter is expected from Figure 6 while the former is not modeled (in the singular re-

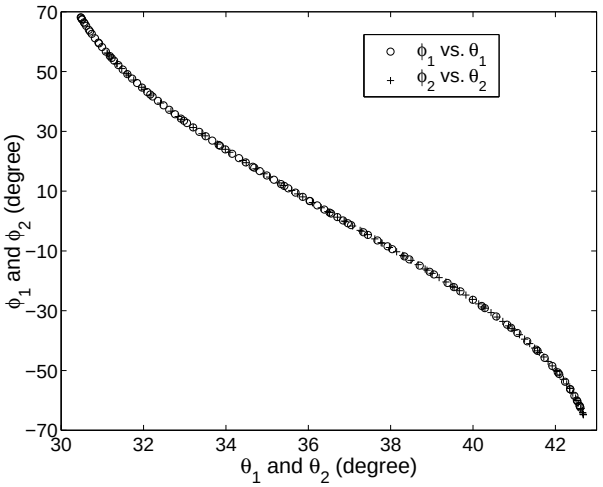

Figure 9: Simulated spar motion due to the given input motions: first spar ('o'), and second spar ('+').

gion in Figure 6), and could be due to the flexible joint mechanism. Furthermore, θ_0 also changes the resonant frequency as can be seen in Figure 15b. This is due to the change in the load on the PZT actuator depending on θ_0.

8 Conclusion

In this paper, a four-bar mechanism with two flexible links is proposed to be used in a micromechanical flying insect thorax design for stroke amplification. PZT and PZN-PT unimorph actuators are utilized at the input link of the four-bar. The kinematics, dynamics and quasi-static force analsis of the proposed wing strcuture is realized. Using laser micromachining and folding techniques, prototype four-bars are constructed, and it is shown that the single four-bar structure can have $90 - 100^o$ stroke motion at 29 Hz with a rigid polyester wing on it. As the future work, the rotational motion of the wing is to be realized with a flexible wing, the resonant frequency of the four-bar mechanism is to be increased by optimizing the wing load, flexure stiffness, output force and N values, and blocking force measurements will be realized and compared with simulations.

Acknowledgements

This work was funded by ONR MURI N00014-98-1-0671, ONR DURIP N00014-99-1-0720 and DARPA. The author would like to thank Ronald S. Fearing for his comments and discussions, and Joseph Yan for helping in assembly and folding process.

Appendix 1: Forward Kinematics

$$
\begin{aligned}
x_1 &= a cos\theta_i \\
y_1 &= a sin\theta_i \\
x_2 &= g - CD \pm \\
&\quad \sqrt{(CD-g)^2 - (1+C^2)(g^2 - b^2 + D^2)} \\
y_2 &= Cx_2 + D \\
C &= \frac{g - a cos\theta_i}{a sin\theta_i}
\end{aligned}
$$

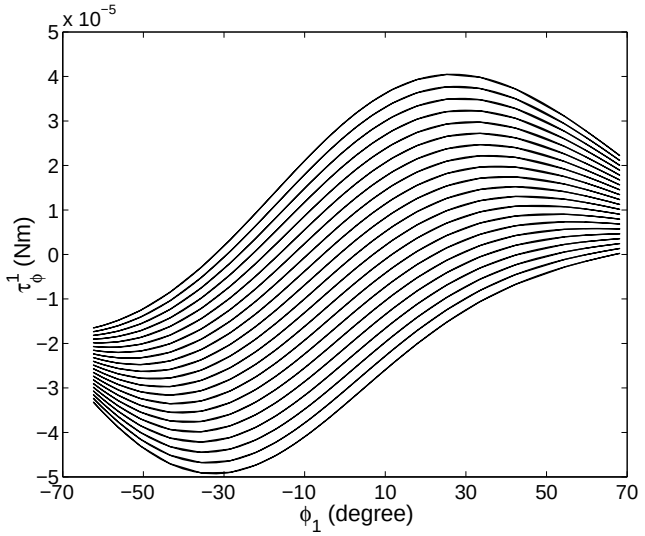

(a)

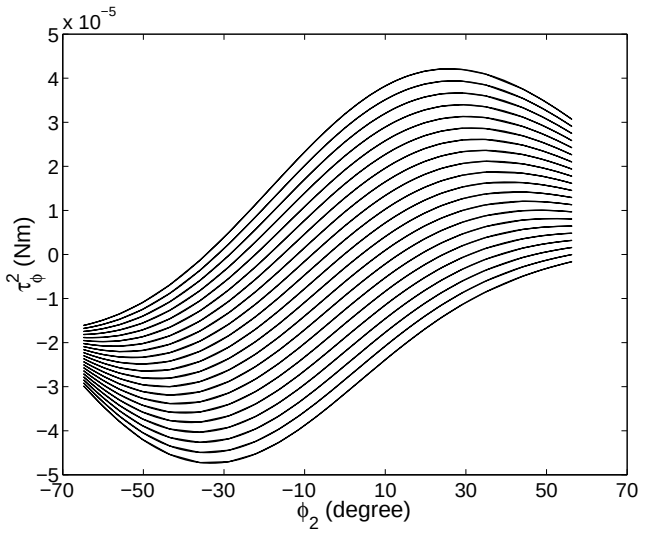

(b)

Figure 10: For electric fields of $E_{1,2} \in [-5, 5]$ $V/\mu m$: (a) τ_ϕ^1 and (b) τ_ϕ^2 blocking torques at the spar ends.

$$
\begin{aligned}
D &= \frac{b^2 - g^2 + a^2 - h^2}{2a sin\theta_i} \\
(X, Y, Z) &= (\frac{x_1 + x_2}{2}, \frac{y_1 + y_2}{2}, \frac{z_1 + z_2}{2}) \\
(X^o, Y^o, Z^o) &= (\frac{x_1^o + x_2^o}{2}, \frac{y_1^o + y_2^o}{2}, \frac{z_1^o + z_2^o}{2}) \\
(x_1, y_1, z_1) &= (x_1^o - L_a cos\phi_1 sin\alpha_1, y_1^o + L_a cos\phi_1 cos\alpha_1, \\
&\quad z_1^o + L_a sin\phi_1) \\
(x_2, y_2, z_2) &= (x_2^o + L_a cos\phi_2 sin\alpha_2, y_2^o + L_a cos\phi_2 cos\alpha_2, \\
&\quad z_2^o + L_a sin\phi_2) \\
(x_1^o, y_1^o, z_1^o) &= (0, \frac{h}{2} sin\phi_1 + a sin\theta_1, g - \frac{h}{2} cos\phi_1 - a cos\theta_1) \\
(x_2^o, y_2^o, z_2^o) &= (L_t, \frac{h}{2} sin\phi_2 + a sin\theta_2, g - \frac{h}{2} cos\phi_2 - a cos\theta_2)
\end{aligned}
$$

where a, b, g and h are the four-bar link lengths for both four-bars as illustrated in Figure 2, and $i = 1, 2$ shows the index number for the four-bars, L_a is the spar length, L_w is the wing cord length, L_t is the separation distance of two four-bars, and α_1 and α_2 are the pan angles of the spars.

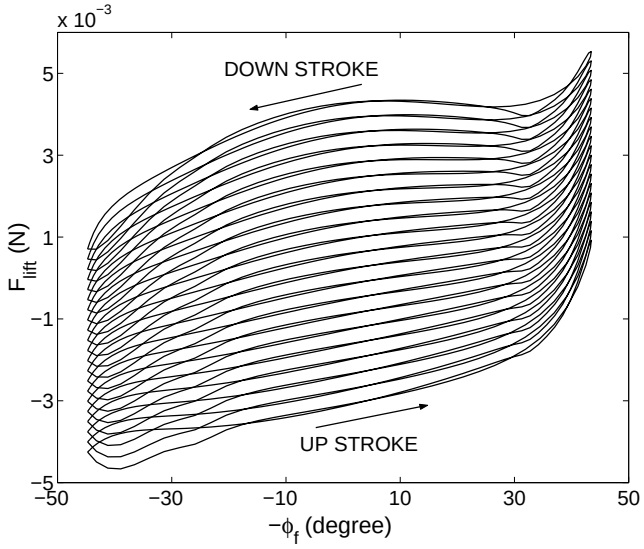

(a)

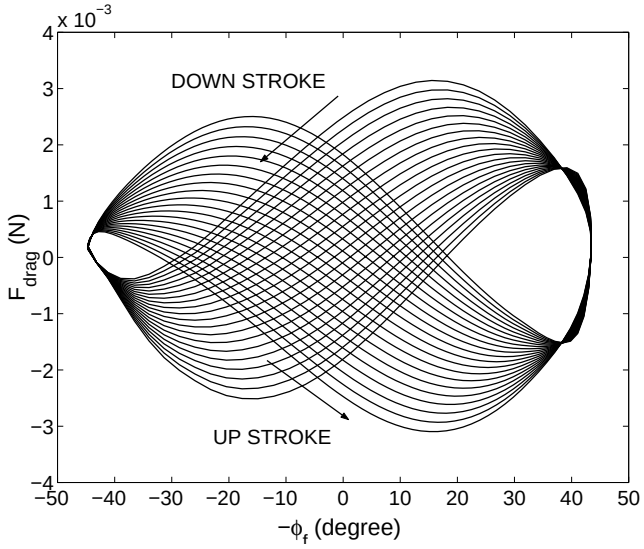

(b)

Figure 11: Spar end lifting and drag forces: (a) F_{lift}, and (b) F_{drag} forces at the wing cord center.

Appendix 2: Inverse Kinematics

$$
\begin{aligned}
\phi_1 &= cos^{-1}\Big(\frac{-BD \pm C\sqrt{-B^2+C^2+D^2}}{C^2+D^2}\Big)\\
\phi_2 &= p-\phi_1\\
p &= 2\phi_f\\
A &= sin\alpha tan\phi_r\\
B &= tan\phi_r L_t/L_a\\
C &= cosp - Asinp + 1\\
D &= A(1+cosp)+sinp\\
\theta_i &= tan^{-1}\Big(\frac{y_1}{x_1}\Big)\\
\psi_i &= tan^{-1}\Big(\frac{y_2}{x_2-g}\Big)\\
x_1 &= \frac{-EF \pm \sqrt{E^2F^2-(F^2-a^2)(1+E^2)}}{1+E^2}\\
y_1 &= Ex_1+F\\
x_2 &= x_1+hcos\phi_i
\end{aligned}
$$

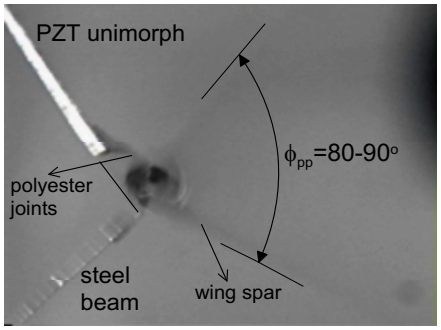

Figure 12: Four-bar and spar motion at resonance (32 Hz) with $\pm 2^o$ unimorph motion input.

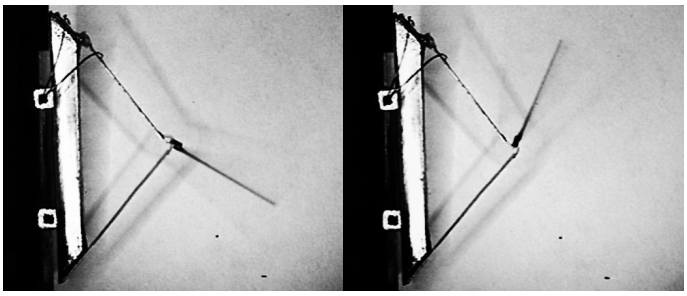

(a) (b)

Figure 13: PZT-5H unimorph actuated spar motion at resonance (33 Hz) with $\pm 2^o$ unimorph motion input: (a) down stroke, (b) up stroke.

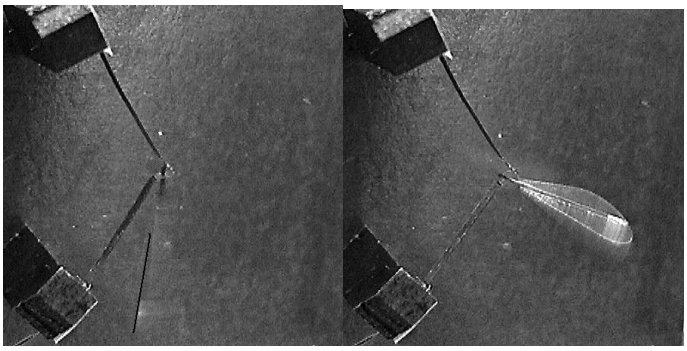

(a) (b)

Figure 14: PZT-5H unimorph actuated wing motion at resonance (29 Hz): (a) down stroke, (b) up stroke.

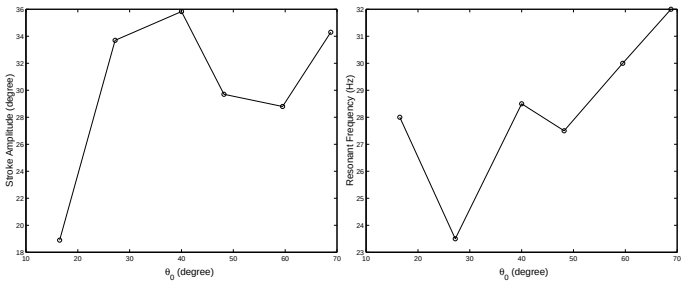

(a) (b)

Figure 15: Effect of θ_0 on (a) stroke amplitude, (b) resonant frequency.

$$
\begin{aligned}
y_2 &= y_1 + h sin\phi_i \\
E &= \frac{-h cos\phi_i + g}{h sin\phi_i} \\
F &= \frac{b^2 + 2gh cos\phi_i - h^2 - g^2 - a^2}{2h sin\phi_i} \ . \qquad (16)
\end{aligned}
$$

For x_1, '$\pm$' becomes '+' for $\phi_i \geq 0$, and '$-$' else.

Appendix 3: Dynamics Parameters

$$
\begin{aligned}
\delta_1 &\approx a\Delta\theta \\
\delta_3 &\approx b\Delta\psi \\
\Delta\theta &= \theta - \theta_0 \\
\Delta\psi &= \psi - \psi_0 \\
\dot{\phi} &= w_2\dot{\theta} \\
\dot{\psi} &= w_3\dot{\theta} \\
w_2 &= \frac{d\phi}{d\theta} = \frac{a sin(\pi + \psi - \theta)}{h sin(\phi - \pi - \psi)} \\
w_3 &= \frac{d\psi}{d\theta} = \frac{a sin(\phi - \theta)}{b sin(\pi + \psi - \phi)} \\
m_t &= m_1^* + m_2 + m_3^* \\
m_2 &= m_\phi + m_s + m_w \approx m_s + m_w \\
I_2 &= I_w + \frac{m_s L_a^2}{3} \\
x &= \frac{(m_s + m_w)L_a/2}{m_\phi + (m_s + m_w)} \approx \frac{L_a}{2} \\
\beta_2 &= tan^{-1}\left(\frac{2x}{h}\right) \\
r_2 &= \frac{h}{2cos\beta_2} \ , \\
A(\theta) &= C_0 + C_1 w_2^2 + C_2 w_3^2 + C_3 w_2 cos(\phi - \theta + \beta_2) \\
\frac{dA}{d\theta} &= 2C_1 w_2 \frac{dw_2}{d\theta} + 2C_2 w_3 \frac{dw_3}{d\theta} + C_3\Big\{\frac{dw_2}{d\theta} cos(\phi - \theta + \delta_2) \\
&\quad -w_2(w_2 - 1) sin(\phi - \theta + \delta_2)\Big\} \\
C_0 &= m_1^* a^2 + m_2 a^2 \\
C_1 &= I_2 \\
C_2 &= m_3^* b^2 \\
C_3 &= 2a r_2 m_2 \\
\frac{dw_2}{d\theta} &= \frac{a(C_4 + C_5)}{h sin^2(\phi - \psi)} \\
\frac{dw_3}{d\theta} &= \frac{a(C_6 + C_7)}{b sin^2(\phi - \psi)} \\
C_4 &= (w_3 - 1) sin(\phi - \psi) cos(\psi - \theta) \\
C_5 &= sin(\psi - \theta) cos(\phi - \psi)(w_3 - w_2) \\
C_6 &= (w_2 - 1) sin(\phi - \psi) cos(\phi - \theta) \\
C_7 &= sin(\phi - \theta) cos(\phi - \psi)(w_3 - w_2) \\
F_0 &= b_1 a^2 + b_3 b^2 w_3^2 + b_w w_2^2 \ , \\
D_0 &= k_1 a^2 \Delta\theta - m_t g a sin\theta \ , \\
D_1 &= k_3 b^2 \Delta\psi \ , \\
D_2 &= -m_3^* g h sin\phi - m_2 g r_2 cos(\beta_2 + \phi)
\end{aligned}
$$

where θ_0 and ψ_0 are the initial link angles, m_w is the wing mass, m_ϕ is the top link mass, and m_s is the spar mass.

References

[1] R. Fearing, K. Chiang, M. Dickinson, D. Pick, M. Sitti, and J. Yan, "Transmission mechanism for a micromechanical flying insect," in *Proc. of the IEEE Int. Conf. on Robotics and Automation*, pp. 1509–1516, San Francisco, CA USA, Apr. 2000.

[2] A. Cox, E. Garcia, and M. Goldfarb, "Actuator development for a flapping microrobotic microaerial vehicle," in *SPIE Microrobotics Symposium*, Nov. 1998, Boston, USA.

[3] I. Shimoyama, H. Miura, K. Suzuki, and Y. Ezura, "Insect-like microrobots with external skeletons," *IEEE Control Systems Magazine*, vol. 13, no. 1, pp. 37–41, 1993.

[4] J. Yan, R. Wood, S. Avandhanula, M. Sitti, and R. Fearing, "Towards flapping wing control for a micromechanical flying insect," in *Proc. of the IEEE Int. Conf. on Robotics and Automation*, Korea, 2001 (to appear).

[5] M. Sitti, D. Campolo, J. Yan, R. Fearing, T. Su, D. Taylor, and T. Sands, "Development of PZT and PZN-PT based unimorph actuators for micromechanical flapping mechanisms," in *Proc. of the IEEE Int. Conf. on Robotics and Automation*, Korea, 2001 (to appear).

[6] B. Pokines and E. Garcia, "A smart material microamplification mechanism fabricated using LIGA," *Smart Mater. Struct.*, vol. 7, pp. 105–112, 1998.

[7] E. Precht and S. Hall, "Design of a high efficiency, large stroke, electromechanical actuator," *Smart Mater. Struct.*, vol. 8, pp. 13–30, 1999.

[8] S. Kota, J. Hetrick, Z. Li, and L. Saggere, "Tailoring unconventional actuators using compliant transmissions: Design methods and applications," *IEEE/ASME Trans. on Mechatronics*, vol. 4, pp. 396–408, Dec. 1999.

[9] S. Kota, J. Hetrick, Z. Li, S. Rodgers, and T. Krygowski, "Synthesizing high-performance compliant stroke amplification systems for MEMS," in *Proc. of the MEMS*, 2000.

[10] A. Cox, D. Monopoli, and M. Goldfarb, "Development of piezoelectrically actuated elastodynamic flapping microaerial devices," in *ASME Adaptive Structures and Material Systems*, pp. 257–262, 1999.

[11] M. Dickinson, F.-O. Lehnman, and S. Sane, "Wing rotation and the aerodynamic basis of insect flight," *Science*, vol. 284, pp. 2085–2104, 18 June 1999.

[12] J. M. McCarthy, *Geometric Design of Linkages*. Springer Verlag, New York, 2000.

[13] Y. Wang and Z.Wang, "A temporal finite element method for the dynamic analysis of flexible mechanisms," *Journal of Sound and Vibration*, vol. 213, no. 3, pp. 569–576, 1998.

[14] M. Karkoub and A. Yigit, "Vibration control of a four-bar mechanism with a flexible coupler link," *Journal of Sound and Vibration*, vol. 222, pp. 171–189, 29 April 1999.

[15] J. Smits and W. Choi, "The constituent equations of piezoelectric heterogenous bimorphs," *IEEE Tran. on Ultrasonics, Ferroelectrics, and Freq. Control*, vol. 38, pp. 256–270, May 1991.

[16] W. Zhang, Q. Li, and L. Guo, "Integrated design of mechanical structure and control algorithm for a programmable four-bar linkage," *IEEE/ASME Trans. on Mechatronics*, vol. 4, pp. 354–362, Dec 1999.